J. Indian Inst. Sci., July–Aug. 1996, **76**, 477–486

A numerical study of axisymmetric vortex breakdown*

A. J. BASU* AND A. KHALILI†
*Jawaharlal Nehru Centre for Advanced Scientific Research, Jakkur, Bangalore 560 064, India, email:*amit@jncasr.ernet.in*
†Max-Planck-Institute for Marine Microbiology, 28239, Bremen, Germany, email:*arzhang@khayam.mpi-mm.uni-bremen.de*

Received on April 30, 1996.

Abstract

In this paper we look at the axisymmetric flow of confined rotating fluid in a cylindrical container. The fluid is set in motion by the rotating bottom lid, and a vortex forms along the axis of the cylinder. In some previous analytical and experimental studies it was suggested that above a critical value of the upstream swirl angle a bubble-type vortex breakdown takes place along the axis, and below that it does not. However, in our present computations, where we compute the swirl angle distribution everywhere in the flow-field, we find no evidence of strong dependence of axisymmetric vortex breakdown on upstream swirl angle, since large swirl angles are seen even in cases where there is no vortex breakdown.

Keywords: Vortex breakdown, swirl angle.

1. Introduction

Vortices exist in nature in nearly all conceivable spatial and temporal scales. From the quantized vortices in liquid helium (spatial dimension of about 10^{-8} cm) to the galaxies (many light years in size), there are vortices in all sizes. They exist sometimes for a fleeting moment, but often for rather large periods of time. They could be life-giving (as in the case of the aortic valve, whose functioning depends critically on vortices[1], and at other times devastating (as in the case of hurricanes).

This dichotomy is also evident in the vortices that form over airplane wings; for example, in a delta-winged aircraft, two strong vortices are formed starting at the leading edge of each wing, and extending far behind the aircraft before they dissipate into the ambient. The parts of the vortices that are over the wing give additional lift to the aircraft, and stabilise it. But the trailing vortices behind a large aircraft can cause problems for smaller aircraft following it, as often happens in busy airports. Of great importance is the phenomenon called 'vortex breakdown'[2] which is known to occur in such swirling flows; this refers to a sudden and explosive enlargement of the vortex core that is sometimes observed (for a review of the vortex breakdown phenomena, see Leibovich[2]). In particular, we will not want vortex breakdown to occur over the wings, but it is desirable

*Text of lecture delivered at the Annual Faculty Meeting of the Jawaharlal Nehru Centre for Advanced Scientific Research at Bangalore on November 11, 1995.

that the aircraft trailing vortices undergo breakdown so that they do not turn into air-traffic hazards. Vortex breakdown is also of critical importance in swirling flows inside nozzles, diffusers and turbomachinery, in addition to tornadoes, etc., in nature.

This, then, is the primary motivation for studying vortex breakdown. It was first reported by Peckham and Atkinson[3] in flow over delta wings at high angles of attack. There have been many subsequent studies: analytical, experimental and numerical, and we will mention a few as we go along. There have been relatively fewer studies of vortex breakdown behind aircraft wings, presumably because of the difficulties involved. Vortex breakdown is known to occur in two main forms: the bubble or axisymmetric type, and the spiral type[4]. We will be looking only at the bubble-type vortex breakdown in this paper.

The main analytical studies of this phenomenon can be attributed to Squire[5], Benjamin[6], and Hall[7]. An early theory of Ludwieg[8] which considered vortex breakdown to be a form of hydrodynamic instability has long been discredited, and we will not go into that here. Squire's theory is based on treating the vortex breakdown phenomenon as standing waves, and he found that the swirl angle ϕ (defined as the ratio of maximum swirl or azimuthal speed, to the axial speed in a rotating flow) is the most important parameter in determining whether vortex breakdown will occur or not. In his study involving inviscid, axisymmetric rotating flow in an infinite domain, he found that a critical value for ϕ between 45 and 50.2° exists for swirling flows where the axial velocity is constant, and the swirl angle has the following distribution.

$$\phi = \tan^{-1}\left[\frac{B}{r}\left(1 - e^{-Cr^2}\right)\right] \tag{1}$$

where r is the radial distance and B and C are some constants. Benjamin, following a different approach involving the critical state theory, arrived at the same conclusion about the existence of a critical upstream swirl angle. Hall's work consists of an analogy of the vortex breakdown phenomenon with boundary-layer separation, and, though interesting, we will not pursue it in this paper.

There have been some experimental verifications of Squire's theory involving the criticality of the upstream swirl angle. Harvey[9] did experiments in rotating pipe flow and measured maximum swirl angle ahead of the vortex breakdown bubble to be at 50.5°, thereby validating Squire's theory. The distribution of the swirl angle measured just ahead of the bubble was found to be of the same form as analysed by Squire.

Axisymmetric vortex breakdown in rotating lid-cylinder geometry (Fig. 1) has received considerable attention ever since the flow-visualization experiments of Escudier[10] who showed rather graphic examples of one, two and three vortex breakdowns as he changed the rotation rate of the lid and the aspect ratio of the cylinder. In his experiments, a stationary cylinder is filled entirely by a viscous liquid, and a lid at one of the ends rotates at a constant angular velocity. What makes this geometry particularly interesting while numerically studying the vortex breakdown phenomenon is the preciseness with which the boundary conditions can be stated, and also that there are only two non-

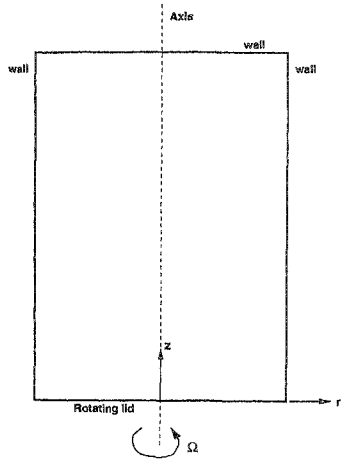

FIG. 1. A schematic of the vertical cross-section of the rotating lid-cylinder geometry.

dimensional parameters governing this flow. There are excellent numerical simulations of this flow (most notably by Lopez[11], among others) that are able to reproduce the experimentally observed features almost identically. In this paper, we attempt to put to test Squire's[5] theory about the existence of a critical swirl angle by means of numerical simulations of vortex breakdown in this geometry.

Escudier's[10] flow-visualization experiments initially received only a lukewarm reception as doubts were raised as to whether the recirculation regions seen in his studies were 'vortex breakdown' or not. Such doubts do not seem to exist anymore, but it just may be so that vortex breakdown as seen in this geometry is different from that in pipe flow, for example. Thus it is important to see whether such a critical value of swirl angle exists even in this flow.

2. Formulation and numerical scheme

In the following, we assume the fluid to be Newtonian and incompressible. The cylinder has a radius R and height H and is completely filled with some viscous fluid (Fig. 1). The lid at the bottom of the cylinder rotates with a uniform angular velocity Ω. The Navier–Stokes equations governing the flow can be written in vector form as

$$\rho\left[\frac{\partial \vec{V}}{\partial t}+(\vec{V}\cdot\nabla)\vec{V}\right]=-\nabla p+\mu\nabla^2\vec{V} \tag{2}$$

which is to be solved along with the continuity equation

$$\nabla\cdot\vec{V}=0. \tag{3}$$

The parameters appearing in eqns (2)–(3) are defined as follows:

ρ = density of the fluid,
μ = molecular viscosity of the fluid,
p = pressure,
$\vec{V}$ = the velocity vector,
∇ = the gradient operator.

If we nondimensionalise using the reference length R and the reference velocity $U = R\Omega$, then we get the following nondimensional variables (denoted by *)

$$\vec{V}^* = \frac{\vec{V}}{U}, p^* = \frac{p}{\rho U^2}, t^* = \frac{t}{(R/U)}, \nabla^* = \nabla R.$$

The nondimensional form of the eqns (2)–(3) may then be written as (after dropping the *)

$$\frac{\partial \vec{V}}{\partial t} + (\vec{V} \cdot \nabla)\vec{V} = -\nabla p + \frac{1}{\mathrm{Re}} \nabla^2 \vec{V} \tag{4}$$

$$\nabla \cdot \vec{V} = 0. \tag{5}$$

Here, Re is the Reynolds number defined as $\mathrm{Re} = \rho \Omega R^2/\mu$. The Reynolds number, along with the aspect ratio $A = H/R$, forms the two governing parameters of this flow.

Because of the geometry used here, we introduce a cylindrical coordinate system (r, θ, z) where r is the radial distance, θ, the azimuthal angle and z, the axial coordinate. Further, we assume the flow to be *axisymmetric* (which is a valid approximation for the moderate Reynolds numbers that we intend to study here), and so, using the equation of continuity (5) we can introduce the streamfunction ψ, defined by

$$u = -\frac{1}{r}\frac{\partial \psi}{\partial z}$$

$$w = \frac{1}{r}\frac{\partial \psi}{\partial r}$$

where u, v and w are the velocity components along r, θ and z, respectively. Pressure can now be eliminated from eqn (4), resulting in the well-known 'vorticity-streamfunction' equations

$$\frac{\partial \eta}{\partial t} + u\frac{\partial \eta}{\partial r} + w\frac{\partial \eta}{\partial z} - \frac{u}{r}\eta - \frac{2v}{r}\frac{\partial v}{\partial z} = \frac{1}{\mathrm{Re}}\left(\frac{\partial^2 \eta}{\partial r^2} + \frac{1}{r^2}\frac{\partial \eta}{\partial r} - \frac{\eta}{r^2} + \frac{\partial^2 \eta}{\partial z^2}\right) \tag{6}$$

$$\frac{\partial v}{\partial t} + u\frac{\partial v}{\partial r} + w\frac{\partial v}{\partial z} + \frac{u}{r}v = \frac{1}{\mathrm{Re}}\left(\frac{\partial^2 v}{\partial r^2} + \frac{1}{r}\frac{\partial v}{\partial r} - \frac{v}{r^2} + \frac{\partial^2 v}{\partial z^2}\right) \tag{7}$$

where η is the azimuthal component of vorticity defined as

$$\eta = \frac{\partial u}{\partial z} - \frac{\partial w}{\partial r}$$

so that

$$-r\eta = \frac{\partial^2 \psi}{\partial r^2} - \frac{1}{r}\frac{\partial \psi}{\partial r} + \frac{\partial^2 \psi}{\partial z^2}. \tag{8}$$

The initial conditions for this problem are

$\psi, v, \eta = 0$ at $t < 0$ for all r and z

$v = r\Omega$ at $t = 0$ for $0 \le r \le R, \quad z = 0$

and the boundary conditions are

$\psi = 0, \quad v = 0, \quad \eta = 0,$ for $r = 0, \quad 0 < z < H$

$\psi = 0, \quad v = 0, \quad \eta = -\frac{1}{r}\frac{\partial^2 \psi}{\partial r^2},$ for $r = R, \quad 0 < z < H$

$\psi = 0, \quad v = r\Omega, \quad \eta = -\frac{1}{r}\frac{\partial^2 \psi}{\partial z^2},$ for $0 \le r \le R \qquad z = 0$

$\psi = 0, \quad v = 0, \quad \eta = -\frac{1}{r}\frac{\partial^2 \psi}{\partial z^2},$ for $0 \le r \le R \qquad z = H.$

The vorticity is evaluated at the boundaries from the computed solution of ψ using a first-order accurate scheme for reasons of stability[11]. Equations (6)–(7) are solved using a high-order accurate compact finite-difference scheme[12]. The scheme is up to sixth-order accurate in the interior and up to third-order accurate at the boundaries. We use a second-order accurate central-difference scheme to solve the Poisson equation for ψ (8). A first-order accurate Euler time-integration scheme is used to integrate the equations of motion to steady state.

3. Results and discussion

In this section, we look at the results obtained using the method above for fluid flow inside a cylindrical container (radius $R = 1$) with a rotating bottom lid. The fluid is at rest initially ($t < 0$). At time $t = 0$, the lid is impulsively set in motion with a uniform angular velocity ($\Omega = 1$). An Ekman boundary layer develops on the rotating lid. This rotating boundary layer acts now as a centrifugal fan, throwing fluid radially outward in a spiralling motion and 'sucking' fluid into it from above. A secondary meridional circulation regime is then set up due to the existence of the solid walls. Above the lid, at first the fluid which is pumped out of the Ekman layer spirals up the cylindrical wall, establishing a Stewartson layer until it reaches the top wall where it is turned and advected towards the central axis. The fluid then spirals down and is pumped back into the Ekman layer.

In our numerical simulations, we have chosen an aspect ratio of 1.5, and three different Reynolds numbers, namely, Re = 1000, 1492 and 2000; these Reynolds numbers are chosen because they lie, respectively, below, within and above the Reynolds number range where vortex breakdown occurs for $A = 1.5$ (see Fig. 7 of Escudier[10] in this

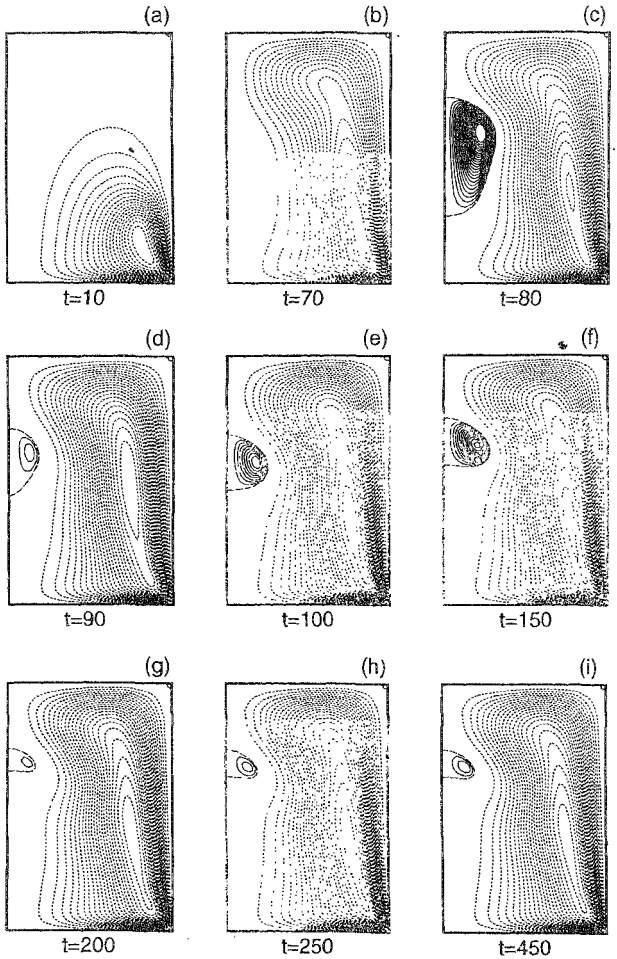

FIG 2. Temporal development of streamfunction contours in the flow at Re= 1492. Only sections from the central axis to the outer walls are shown. The nondimensional times for the figures are: (*a*) 10, (*b*) 70, (*c*) 80, (*d*) 90, (*e*) 100, (*f*) 150, (*g*) 200, (*h*) 250, (*i*) 450. There are 20 equispaced contours between $\psi = 0$ and $-.01$, and another 20 equispaced contours between $\psi = 0$ and 2×10^{-4}. The positive streamlines are shown in solid lines, whereas the negative ones are shown dashed; the zero streamlines are shown by long dashed lines.

context). These Reynolds numbers can be achieved, for instance, by variations of the angular velocity of the rotating lid. Thus, when we start from rest and slowly increase Ω, flow develops inside the cylindrical container but no vortex breakdown bubble can be seen till after Re = 1050 or so. As Reynolds number is increased further, a bubble-type vortex breakdown occurs at the axis, but it disappears again around Re = 1900 or so. So, at Re = 1000, the breakdown bubble is yet to appear; at Re = 1492 there is a recirculation region at the axis, and at Re = 2000 the bubble has disappeared. The Re = 1492 case was chosen specifically so that comparisons can be made with the visualizations of Escudier. The results presented here use a 61×91 uniform grid. Test computations using 81×121 grid showed no perceptible difference in any computed quantity.

We present the temporal development of the flow for the Re = 1492 case in Fig. 2. Since the flow is axisymmetric, in all the following figures we show only sections bounded by the central axis and the outer walls (equivalent to the region in the right half of Fig. 1). The streamfunctions are shown using equispaced contour levels on either side of $\psi = 0$, so that the breakdown bubble can be seen easily (the flow in the bubble is very weak, and therefore will not be visible if the usual equispaced contours are drawn). Note that Fig. 2, etc., are not in uniform time-sequence; this was deliberately done so that important events during development of the flow can be captured. The breakdown bubble appears between (nondimensional) times $t = 70$ and $t = 80$. The bubble oscillates in size and shape (but never completely disappears) for considerable time before settling down to a steady state by $t = 450$, as can be seen from these figures.

In Fig. 3, we present the computed streamfunctions for the three Reynolds numbers after steady states have been achieved in each case through numerical integration. Nondimensional times to reach steady states are 250, 450 and 500, respectively, for the cases with Reynolds numbers 1000, 1492 and 2000 (a time-step of 0.025 was used in all

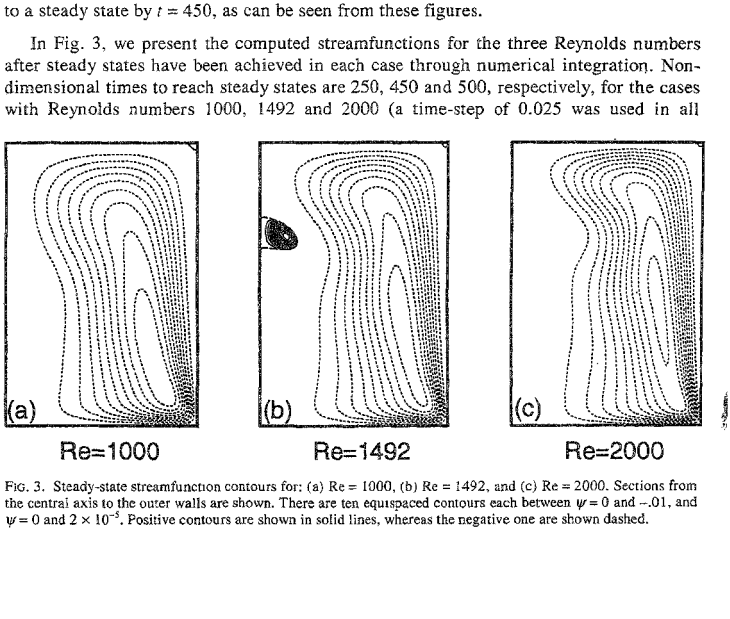

FIG. 3. Steady-state streamfunction contours for: (a) Re = 1000, (b) Re = 1492, and (c) Re = 2000. Sections from the central axis to the outer walls are shown. There are ten equispaced contours each between $\psi = 0$ and $-.01$, and $\psi = 0$ and 2×10^{-5}. Positive contours are shown in solid lines, whereas the negative one are shown dashed.

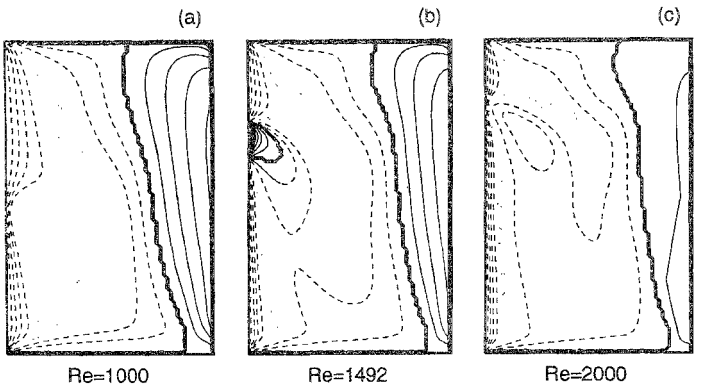

FIG 4. Computed distributions of swirl angle ϕ (in degrees) in the flow for: (a) Re = 1000, (b) Re = 1492, (c) Re = 2000. Sections from the central axis to the outer walls are shown. The contour levels are from $\phi = -90$ to +90 at intervals of 10. Positive contours are shown in solid lines, whereas the negative one are shown dashed. The regions between $\phi = -50$ and -60 are shown filled in grey.

cases). Figure 3(b) for Re = 1492 can actually be compared with Fig. 3(d) of Escudier's[10] flow visualization pictures. The similarities with the experimental flow-visualization pictures confirm the accuracy of the present calculations. We can also see that there are perceptible waves in the flow-field for both Re = 1000 and Re = 2000, but that there is no recirculation region at the axis (in conformity with Escudier's results). The recirculation zone in Fig. 3(b) is very weak, and has near-stagnant fluid as has been found in experiments too.

In Fig. 4, we have the computed swirl angle distributions over the entire flow-field for the three different Reynolds numbers. The swirl angle ϕ is defined as

$$\phi = \tan^{-1}(v/w).$$

The regions between $\phi = -50$ and $-60°$ are filled in grey in order to highlight them. From Squire's theory and also from various experiments in pipe flow, one should expect a region just ahead of the breakdown bubble where the absolute value of ϕ is greater than 50. From the figure, it is clear that though such a region for Re = 1492 exists, it is not close enough to the axis of rotation to be unambiguously called the 'upstream of the bubble'. Moreover, one can see that such regions of high swirl exist even at Re = 1000 and 2000, and that these regions are closer to the axis than that for Re = 1492. If the criticality condition of Squire[5] was necessary and sufficient for the existence of vortex breakdown in this flow, one would expect no large swirl angles around the axis for Re = 1000 and 2000.

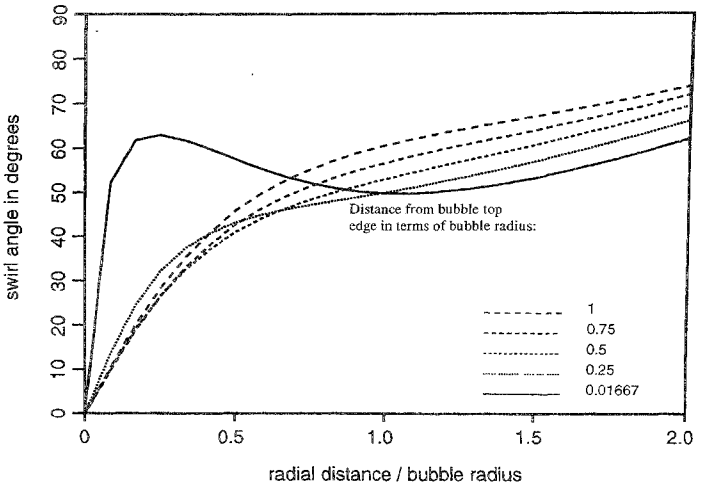

FIG. 5. Computed distribution of swirl angle ϕ (in degrees) at various distances upstream of the vortex breakdown bubble for RE = 1492.

To compare with the results of Harvey[9], we take a closer look at the distribution of the swirl angle just upstream of the breakdown bubble. In Fig. 5, we present the distribution at different upstream distances as a function of the radial distance r. As can be seen, the distribution (for small r) of the swirl angle ϕ upstream of the breakdown bubble changes very rapidly from the classical form given in eqn (1) close to the bubble, to a near-logarithmic form a little distance away.

Thus it appears that a region of large swirl (swirl angle greater than 50°) is not a sufficient condition for vortex breakdown, although it may be a necessary one. While this observation is valid for the rotating lid-cylinder geometry, we do not yet know whether similar behaviour can be observed in swirling pipe flows or flow over delta wings.

4. Conclusion

We have computed the distribution of swirl angle over the entire flow-field inside a cylindrical container with a rotating bottom lid. We find that existence of upstream swirl angle greater than some critical value (as suggested by several investigators) is not a sufficient condition for the existence of a vortex breakdown bubble, even though it is likely to be a necessary one. This finding points to the possibility that the precise character of vortex breakdown may be very sensitive to the actual flow situation, especially on

the boundary conditions imposed, since the boundary conditions in the actual experiments (rotating pipe flow) and analytical solutions (infinite rotating disk) were different from that in the present numerical simulation.

Acknowledgements

The authors would like to thank Prof. Roddam Narasimha for illuminating discussions on this subject.

References

1. BELLHOUSE, B. J. AND TALBOT, L. *J. Fluid Mech.*, 1969, **35**, 721.
2. LEIBOVICH, S. *A Rev. Fluid Mech.*, 1978, **10**, 221–246.
3. PECKHAM, D. H. AND ATKINSON, S. A. *Aero. Res Coun. CP* 508, 1957.
4. SARPAKAYA, T. *J Fluid Mech.*, 1971, **45**, 545–559.
5. SQUIRE, H. B. *Aero. Dept Report 102*, Imperial College, London, 1960.
6. BENJAMIN, T. B. *J. Fluid Mech.*, 1967, **28**, 65–84.
7. HALL, M. G. *A. Rev. Fluid Mech.*, 1972, **4**, 195–218.
8. LUDWIEG, H. *Z. Flugwiss.*, 1962, **10**, 242–249.
9. HARVEY, J. K. *J. Fluid Mech.*, 1962, **14**, 585–592
10. ESCUDIER, M. P. *Exp. Fluids*, 1984, **2**, 189–196.
11. LOPEZ, J. M. *J Fluid Mech.*, 1990, **221**, 533–552.
12. LELE, S. K. *J Computational Phys.*, 1992, **103**, 16–42.